https://dx.doi.org/10.1016/j.polymdegradstab.2022.110002
This is the Pre-Published Version.

Synthesis of magnolol-derived bisphosphate for fabrication of bismaleimide resins with intrinsic anti-flammability and smoke suppression

Wenwen Guo [a, b, c, *], Fuwei Liang [a], Shun Chen [a], Diantang Zhang [a], Wenbing Li [a], Kun Qian [a], Yang Xu [a], Bin Fei [b, *]

[a] Key Laboratory of Eco-textiles, Ministry of Education, College of Textile Science and Engineering, Jiangnan University, 1800 Lihu Avenue, Wuxi, Jiangsu 214122, China.

[b] Institute of Textiles and Clothing, The Hong Kong Polytechnic University, Hong Kong, China.

[c] State Key Laboratory of Fire Science, University of Science and Technology of China, 96 Jinzhai Road, Hefei, Anhui 230026, China.

*Corresponding Author: Wenwen Guo, Bin Fei. Email: guoww@jiangnan.edu.cn (W. Guo), bin.fei@polyu.edu.hk (B. Fei).

Abstract

A magnolol-derived bisphosphate (MBDPP) was successfully synthesized from the substitution reaction between magnolol and diphenyl phosphoryl chloride. MBDPP was subsequently applied for the fabrication of intrinsically anti-flammable bismaleimide (BMI) thermosets. The effect of MBDPP on the curing kinetics of BMI systems was investigated by the non-isothermal DSC technology, showing that the addition of MBDPP increased the reaction activation energy of the BMI system owing to the steric hindrance of MBDPP. With only 2 wt% of MBDPP, the BMI thermoset achieved the LOI of 35.0% and UL-94 V-0 grade. Besides, the PHRR, MARHE, THE, TSP and mean

© 2022. This manuscript version is made available under the CC-BY-NC-ND 4.0 license http://creativecommons.org/licenses/by-nc-nd/4.0/.

SEA of the BMI thermoset with 2 wt% of MBDPP were declined by 26%, 33%, 27%, 34% and 50%, respectively, compared to those of the unmodified BMI. The enhanced anti-flammability and smoke suppression performances of the BMI thermosets were attributed to the formation of an intact, expansive and thermally resistant char layer by the presence of MBDPP. Such a char layer effectively blocked the transportation of combustible degradation products to the flame and the thermal radiation of heat to the polymer matrix, so as to slow down the heat release rate and smoke emission.

Keywords: Magnolol; Bismaleimide; Intrinsic anti-flammability; Smoke suppression

Graphical Abstract

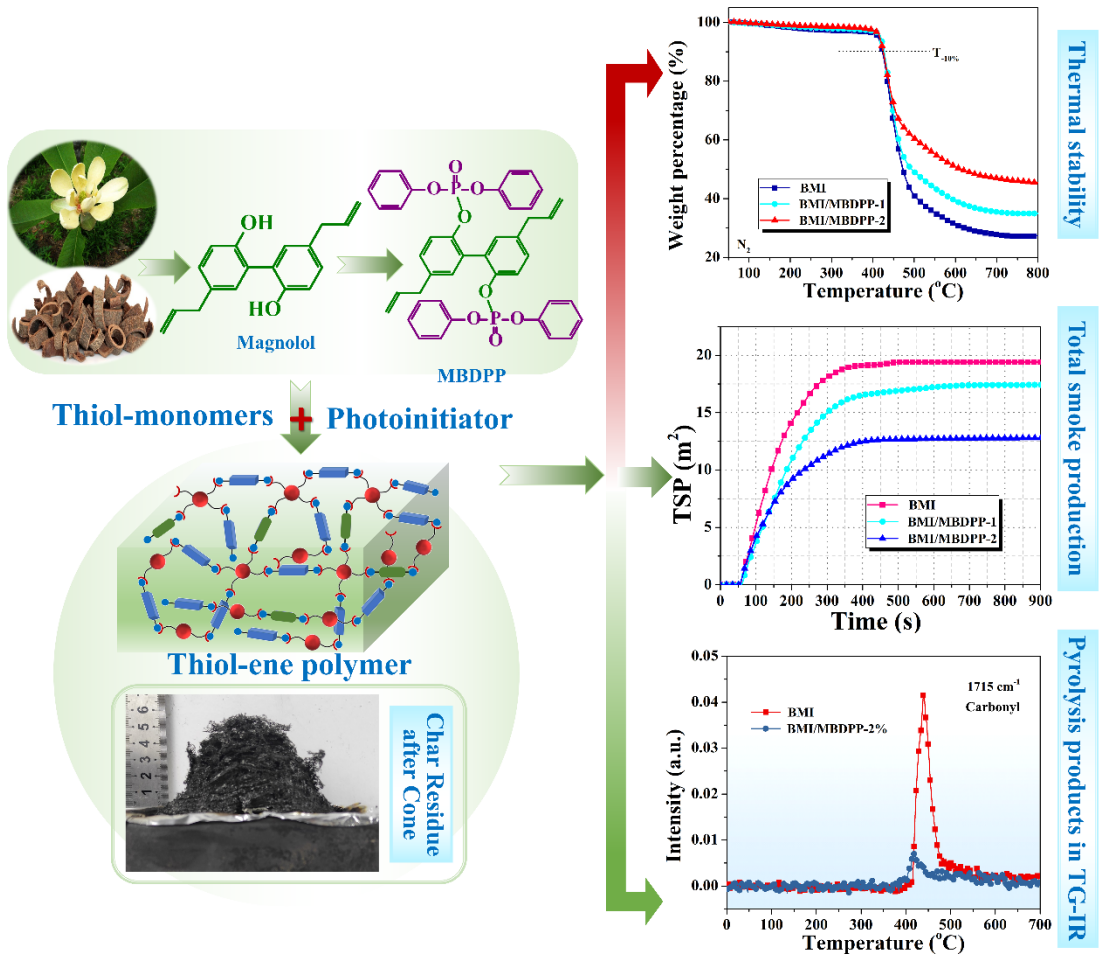

1. Introduction

Bismaleimide resin (BMI) is one kind of bifunctional compound with maleimide as active terminal groups, which is derived from polyimide resin [1, 2]. BMI integrates the advantages of high-temperature thermal stability of polyimide resin and the easy processability of epoxy resin. Besides, it also possesses excellent electrical insulation, weather resistance and outstanding dimensional stability. Therefore, BMI has been widely applied as the matrix resin of high-performance composites, high-temperature insulation materials and high-temperature adhesives, in the fields of aerospace, electronic appliances, transportation, and so on. However, the high crosslinking density and rigid molecular structure of BMI lead to the disadvantage of the high brittleness of the cured networks. In order to overcome this disadvantage, allyl compounds are usually used for copolymerization to toughen BMI [3]. The introduction of allyl compounds will often sacrifice the flame retardant performance of BMI, improving the fire risk of BMI including heat hazard and smoke hazard. Therefore, improving the fire safety of BMI is the key factor to expand its applications.

Presently, BMI is mainly flame retarded by physical blending and chemical copolymerization. The physical blending method is mainly to incorporate flame retardant additives to modify BMI by melting or solution blending. For example, several inorganic nano-materials or hybrid materials including phosphorus-containing polyhedral oligomeric silsesquioxane (POSS) [4], phosphorus-containing POSS modified graphene oxide [5], combination of ionic liquid functionalized graphene and ammonium polyphosphate [6], MoS_2@TiO_2 [7], g-C_3N_4@polyphosphazene [8], have been applied to the flame retardant modification of BMI. Although they have achieved

a good flame retardant effect, these flame retardant additives have two disadvantages: first, the satisfactory flame retardant effect can be achieved only with high addition amount, and the flame retardant efficiency still needs to be improved; Second, inorganic nano-materials or hybrid materials are prone to agglomerate during processing, so they are not suitable for large-scale applications. The chemical copolymerization method is mainly to introduce monomers with flame retardant elements (such as phosphorus, nitrogen, silicon, etc.) and reactive functional groups (such as allyl, amino, etc.) into BMI cross-linking networks for flame retardant modification by covalent bonding. The advantages of the reactive-type flame retardant method over the additive-type one lie in the better compatibility between monomers and BMI matrix and higher flame retardant efficiency. For example, Yan's group synthesized a phosphorus-containing diallyl bisphenol A (P-DBA) and copolymerized it into the BMI system [9]. With the increase of P-DBA content, the UL-94 grade of BMI resin improved from V-1 to V-0, but the initial thermal stability deteriorated. Gu's group synthesized a phosphorus-containing polysiloxane (PN-PSQ) with amino terminal groups [10], and the oxygen index and mean heat release rate of the BMI system containing 5 wt% PN-PSQ were 1.6 times and 58% of that of the unmodified BMI, respectively. In another work, Gu's group also synthesized a phosphorus-containing polysiloxane (HPSi-IFR) [11]. With the addition of 20 wt% HPSi-IFR, the oxygen index of the BMI system was increased to 33.8% from 26.0% for the unmodified BMI, and the UL-94 performance was not mentioned. So, the development of highly efficient flame retardant BMI remains a challenging task.

In recent years, the fabrication of flame retardant polymers from bio-based resources has attracted extensive interest owing to the increasing awareness of sustainable development. Under this background, some bio-based flame retardant monomers have been developed for BMI. Wu *et al.* synthesized a hexa(eugenol)cyclotriphosphazene (HECTP) from eugenol, which endowed the BMI matrix with superior thermal stability at high temperature and outstanding flame retardant behaviors [12]. Wang *et al.* also fabricated an allyl functionalized phosphazene (HECP) from eugenol, which effectively suppressed the heat release and smoke emission of BMI [13]. However, there are very few reports regarding bio-based flame retardant BMI systems.

Magnolol could be extracted from Magnolia Officinalis, which has a strong antibacterial effect. In its unique structure, magnolol has two phenolic hydroxyl and two allyl groups, which makes it a versatile platform for the fabrication of diverse bio-based polymers or additives. Very recently, magnolol has been utilized to prepare flame retardant epoxy resins [14, 15] and polybenzoxazine resins [16]. These studies convince us that magnolol is a promising building block for fabricating high performance BMI resins. In this work, we synthesized a magnolol-derived bisphosphate (MBDPP) as a copolymerization monomer for the fabrication of BMI resins with intrinsic anti-flammability and smoke suppression. The influence of MBDPP on the curing kinetics, thermomechanical property, thermal decomposition and anti-flammability of the BMI resins was investigated. The flame retardant mechanisms of the BMI/MBDPP system were clarified eventually.

2. Experimental section

2.1. Materials

Magnolol, diphenyl phosphoryl chloride (DPPC), triethylamine, dichloromethane, 2, 2'-diallyl bisphenol A (DBA), 4, 4'-bismaleimidodiphenylmethane (BDM) and anhydrous sodium sulfate were purchased from Aladdin Chemical, China. All the reagents were used as received.

2.2. Synthesis of magnolol-derived bis(diphenyl phosphate) (MBDPP)

Magnolol (26.63 g, 0.10 mol), triethylamine (20.24 g, 0.20 mol) and dichloromethane (100 mL) were added into a 250 mL flask under ice water bath. The mixture was stirred vigorously until a homogenous solution was obtained. Subsequently, a dichloromethane solution (50 mL) containing DPPC (53.72 g, 0.20 mol) was dropped into the above mixture in an icing bath. The reaction system was kept at 0 °C for 3 h and 50 °C for another 3 h. Afterward, the precipitate was removed by filtration, and then the filtrate was washed with distilled water (100 mL × 5). The organic layer was separated and dried with anhydrous sodium sulfate overnight. The solvent was removed by vacuum distillation. The yellow viscous liquid was yielded and dried in a vacuum oven (60 °C) overnight. The synthetic process of MBDPP was depicted in scheme 1a.

2.3. Fabrication of MBDPP-derived BMIs

The fabrication of MBDPP-derived BMIs is diagrammatically illustrated in Scheme 1b. Specifically, the preparation procedure of BMI material with 1.0 wt% MBDPP was described as below: BDM (58.0 g), DBA (41.0 g) and MBDPP (1.0 g) were blended in a beaker at 150 °C for about 30 min to obtain a homogeneous mixture. Subsequently, the mixture was transferred to a PFTE mold immediately. The curing procedure was set

as 150 °C for 2 h, 180 °C for 2 h, 210 °C for 2 h, and 240 °C for 2 h. After the completion of the curing procedure, the BMI samples were cooled down to ambient temperature and named after BMI/MBDPP-1. The BMIs containing 2.0 wt% MBDPP were fabricated using the same procedure and coded as BMI/MBDPP-2. The unmodified BMI was also prepared as a control sample using the same way.

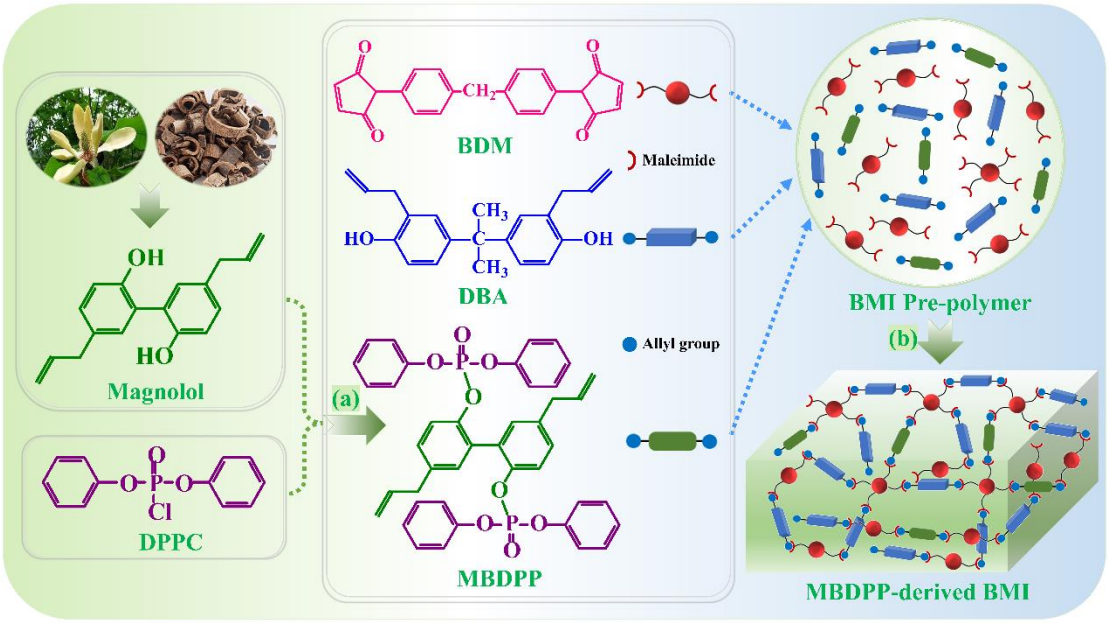

Scheme 1. Diagrammatical illustration of (a) the synthetic route of MBDPP and (b) the fabrication of MBDPP-derived BMIs

2.4. Characterization

Nuclear magnetic resonance (NMR) spectrometer (Bruker AVANCE III 400 MHz) was utilized to characterize the chemical structure of the target product, with deuterated chloroform as solvent.

Fourier-transform infrared (FTIR) spectrometer (Nicolet 6700) was employed to characterize the chemical structure of the target product using the KBr disc method.

Differential scanning calorimetry (DSC, TA Q2000) was used to explore the curing kinetics of the samples at diverse heating rates of 5, 10, 15 and 20 °C/min.

Dynamic mechanical analyzer (TA Q800) was used to analyze the thermomechanical property of the specimens (dimensions: 35 mm × 10 mm × 3 mm) at a heating rate of 5 °C/min from 25 to 350 °C.

Thermogravimetric analyzer (MetelerToledo 1100SF) was implemented to investigate the thermal decomposition behaviors under air and nitrogen atmosphere. The specimens were heated at a rate of 20 °C/min from 50 to 800 °C.

The limiting oxygen index (LOI) tester (PX-01-005) was utilized to determine the LOI value of the specimens (dimensions: 100 mm × 6.5 mm × 3 mm) according to the standard ASTM D2863-17a.

The burning chamber (PX-03-001) was applied to measure the UL-94 vertical combustion performances of the specimens (dimensions: 100 mm × 13 mm × 3 mm).

Cone calorimeter (VOUCH 6810) was carried out to study the flammability of the specimens (dimensions: 100 mm × 100 mm × 3 mm) according to the standard ISO5660. The heat flux used was 50 kW/m^2.

Scanning electron microscope (SEM, HITACHI SU-1510) was utilized to observe the morphology of the char residues.

X-ray photoelectron spectrometer (XPS, Axis Ultra DLD) was applied to explore the elemental analysis of the char residues using Al K_α source (h_ν = 1486.6 eV).

Laser confocal Raman microscope (LabRAM HR Evolution) was employed to study the graphitized structure of the char residues.

Thermogravimetric analyzer (TA Q5000) combined with FTIR spectrometer (Nicolet 6700) system was applied to identify the pyrolysis products of the specimens. The

specimens were heated at a rate of 20 °C/min from 50 to 700 °C. The pyrolysis products were sent to the gas chamber of the FTIR spectrometer through a heated stainless steel tube (the temperature was kept at 280 °C).

3. Results and discussion

3.1 Structural Characterization

MBDPP was synthesized from the substitution reaction between magnolol and DPPC. Fig. 1a gives the ^{1}H-NMR spectrum of MBDPP. The multiple peaks in the chemical shift ranged from 7.12 to 7.42 ppm were allocated to the aromatic protons of the benzene rings. The peaks at around 5.98 and 5.10 ppm were assigned to the protons of the C=C bond (marked by a and b). The peak at around 3.43 ppm was assigned to the methylene protons of the allyl group (marked by c). Fig. 1b gives the ^{13}C-NMR spectrum of MBDPP. All the peaks matched well with the designed molecular structure of MBDPP, demonstrating the successful synthesis of MBDPP. Fig. 1c displays the FTIR spectrum of MBDPP. The characteristic peak at 3071 cm^{-1} was ascribed to the stretching vibrations of the C-H bond in the benzene rings. The characteristic peak at 1637 cm^{-1} was assigned to the vibrations of the C=C bond in the allyl group. The characteristic peaks at 1590 and 1487 cm^{-1} were corresponding to the skeleton vibration of the benzene rings. The characteristic peaks at 1187 and 960 cm^{-1} were allocated to P=O and P-O-Ph, respectively, further manifesting the successful introduction of diphenyl phosphate. The real-time FTIR spectra were recorded to monitor the curing reaction process of BMI/MBDPP-2 systems. As shown in Fig. 1d, several functional groups could be clearly identified by the characteristic bands: the absorption band at

1715 cm^{-1} was assigned to the carbonyl stretching of maleimide rings; the absorption band at 1635 cm^{-1} was allocated to the allyl C═C stretching of DBA and MBDPP; the absorption bands at 914 and 826 cm^{-1} were due to the out-of-plane bending of allyl C═C-H and maleimide ═C-H, respectively [17]. With proceeding the curing process, the intensity of these absorption bands became much weaker even disappeared, which demonstrated the successful occurrence of the Ene and Diels-Alder reactions among BDM, DBA and MBDPP to form the cured networks [18].

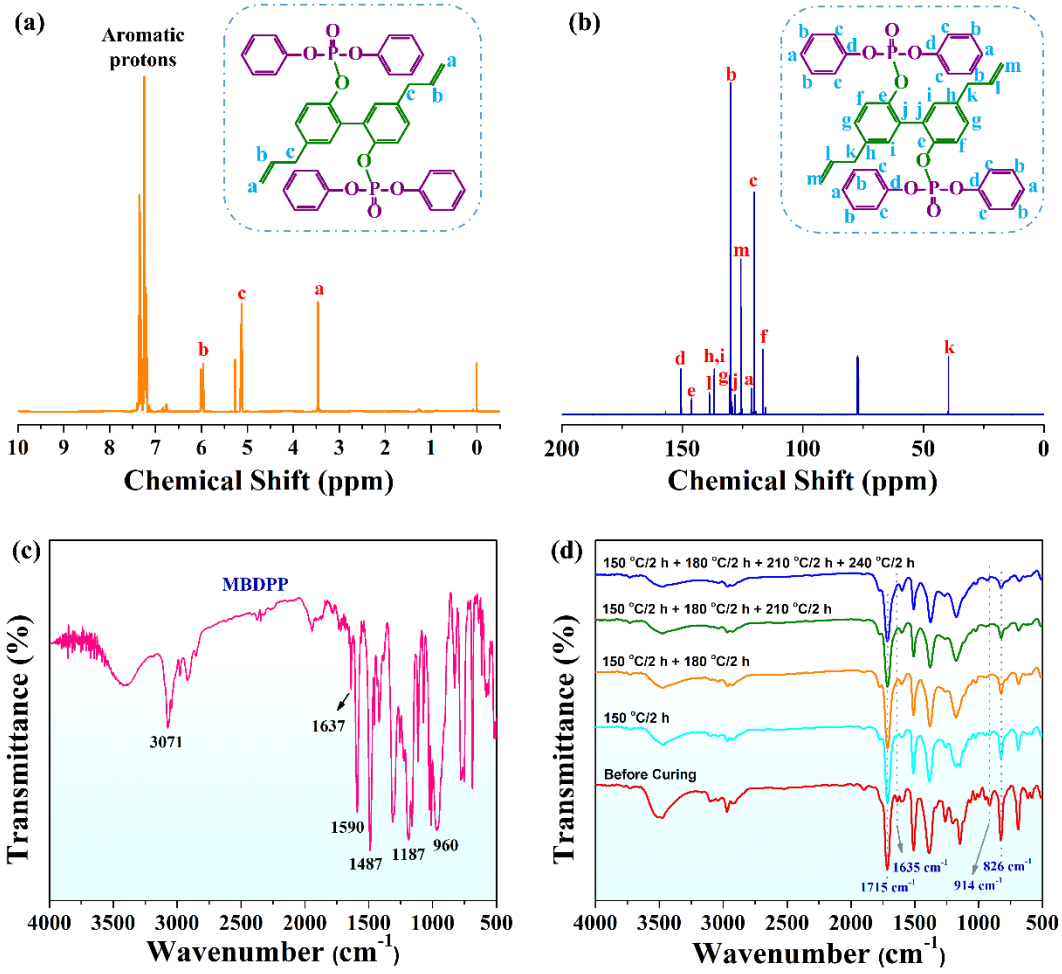

Fig. 1 (a) Proton and (b) carbon NMR spectra of MBDPP; (c) FTIR spectrum of MBDPP; (d) The real-time FTIR spectra of BMI/MBDPP-2 systems during the curing reaction process

3.2 Curing kinetics

The non-isothermal DSC technology was employed to explore the curing kinetics of BMI and BMI/MBDPP-2 systems. Fig. 2 illustrates the non-isothermal DSC profiles of BMI and BMI/MBDPP-2 systems at diverse heating rates of 5, 10, 15 and 20 °C/min, and the relating DSC curing parameters are summarized in Table 1. It can be found that from Fig. 2 that there were two exothermic peaks for both BMI (Fig. 2a) and BMI/MBDPP-2 (Fig. 2b) systems, indicating the presence of two reaction stages. The first exothermic peak was ascribed to the Ene reaction between the allyl group in DBA with the C=C bond in maleimide ring, while the second one was assigned to the Diels–Adler reaction at high temperatures [19, 20]. From the exothermic peak, the initial curing temperature (T_i), peak temperature (T_p), terminated temperature (T_{end}), and curing enthalpy (ΔH) are determined. It was found from Table 1 that the T_i, T_p, and T_{end} shifted to higher temperatures with the increment of the heating rate. This was because the time for the molecular movement was insufficient at a higher heating rate, resulting in the lower reaction possibility of the functional groups in the curing system [21]. The apparent activation energy (E_a) of curing reaction is calculated according to Kissinger's equation[22, 23]:

$$ln\left(\frac{\beta}{T_p^2}\right) = ln\left(\frac{AR}{E_a}\right) - \frac{E_a}{RT_p}$$

where β, A, and R mean the heating rate, the pre-exponential factor, and the ideal gas constant (8.314 $J \cdot mol^{-1} \cdot K^{-1}$), respectively. E_a is obtained from the slope ($-E_a/R$) of the linear fitting plots of $\ln(\beta/T_p^2)$ *versus* $1/T_p$ (Fig. 2c). The calculated E_a values of BMI and BMI/MBDPP-2 systems were 79.08 and 83.07 kJ/mol, respectively. The addition

of MBDPP increased the reaction activation energy of the BMI system, which is owing to the slow diffusion rate of the curing reaction system caused by the steric hindrance of MBDPP.

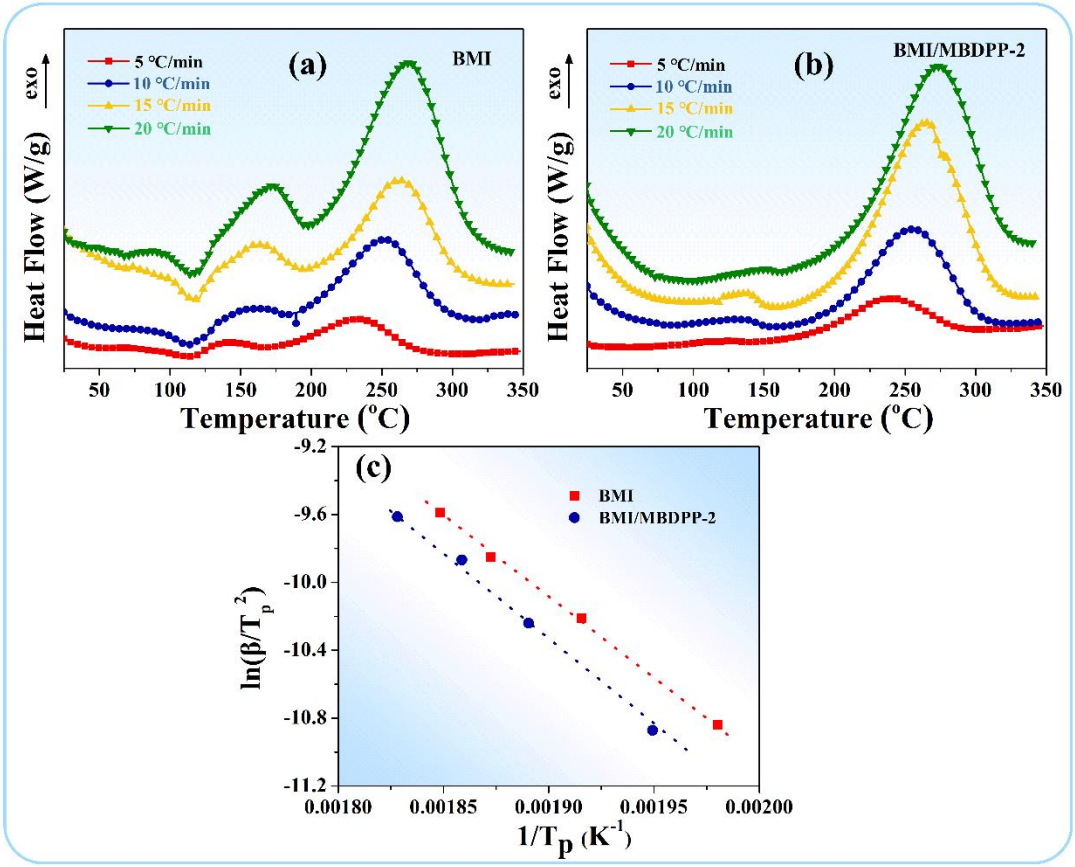

Fig. 2 The non-isothermal DSC profiles of (a) BMI and (b) BMI/MBDPP-2 systems at diverse heating rates; (c) The linear fitting plots of $\ln(\beta/T_p^2)$ *versus* $1/T_p$ of BMI and BMI/MBDPP-2 systems

Table 1. DSC curing parameters of BMI and BMI/MBDPP-2 systems

Sample	β (ºC/min)	T_{onset} (°C)	T_p (°C)	T_{end} (°C)	ΔH (J/g)	E_a (kJ/mol)
BMI	5	118	232	294	406.9	79.08
	10	120	249	310	427.4	
	15	122	261	322	395.7	
	20	124	268	335	368.1	
BMI/MBDPP-2	5	85	240	296	334.5	83.07
	10	91	256	315	294.4	
	15	110	265	329	311.8	
	20	115	274	335	361.0	

3.3 Thermal decomposition behaviors

Fig. 3 shows the TGA and differential TGA (DTG) curves of the bismaleimide samples under nitrogen and air. Several characteristic parameters containing temperatures at 10%, 50% weigh loss ($T_{-10\%}$ and $T_{-50\%}$), maximum mass loss rate (T_{max}) and char yields at 800 ℃ (C800) were summarized in Table 2. As can be seen from Fig. 3a, the bismaleimide sample showed only one major mass loss stage under nitrogen. The mass of unmodified bismaleimide decreased rapidly in the temperature range from 400 to 510 ℃, and the mass loss was up to 60%, which was attributed to the thermal degradation of the cured bismaleimide three-dimensional network into a series of small molecular volatile products. The main mass loss stages of BMI/MBDPP-1 and BMI/MBDPP-2 also occurred in the temperature range from 400 to 510 ℃, with a mass

loss of 50% and 40%, respectively. Compared with the unmodified bismaleimide, the degradation products of MBDPP (such as phosphoric acid compounds) can promote the dehydration, cyclization, and carbonization of the BMI matrix, so as to improve the char formation of BMI at high temperature. The char residues of BMI/MBDPP-1 and BMI/MBDPP-2 at 800 ℃ are 35.0% and 45.5%, respectively, which was significantly higher than that of unmodified BMI (27.4%). As can be seen from Fig. 3b, the maximum mass loss rate of BMI/MBDPP-1 and BMI/MBDPP-2 was significantly lower than that of the unmodified BMI, indicating that the char layer formed during the pyrolysis of flame retardant modified bismaleimide can effectively inhibit the mass loss rate. Under air, the bismaleimide samples showed two main mass loss stages (Fig. 3c and 3d). The first mass loss stage corresponded to the degradation of the cured bismaleimide three-dimensional network when heated, and the second mass loss stage was related to the further oxidative degradation of the char under the action of oxygen. Similar to nitrogen, the addition of MBDPP greatly improved the thermal stability of bismaleimide at high temperatures. Specifically, the temperature at 50% weight loss ($T_{-50\%}$) of BMI/MBDPP-2 was about 35 °C higher than that of unmodified BMI. However, due to oxidation, the char yield of the bismaleimide samples in air was significantly lower than that in nitrogen. The above results showed that MBDPP has good catalytic charring performance, which is conducive to reducing the mass loss rate (escape of combustible gas) during combustion and improving the flame retardant performance.

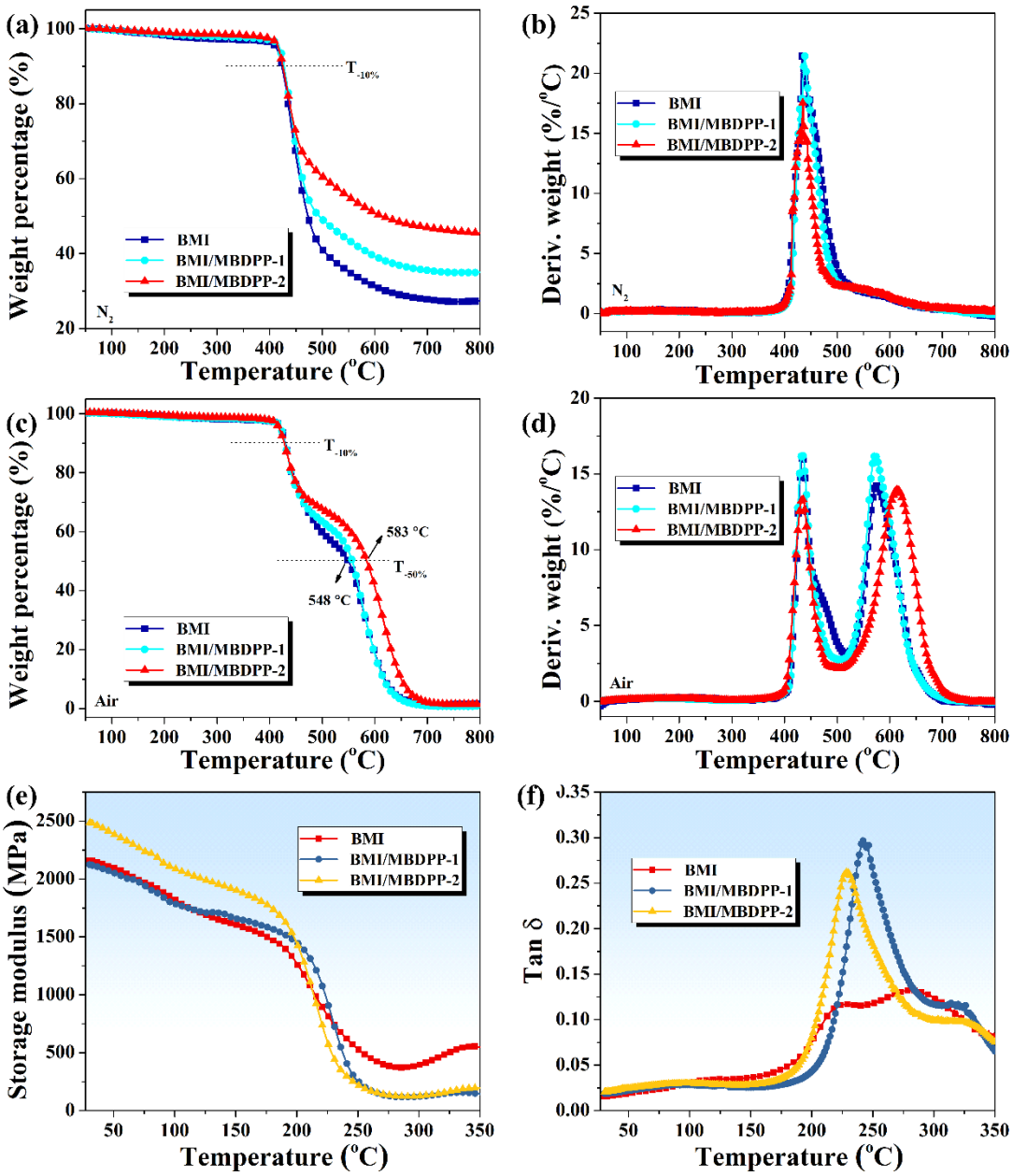

Fig. 3 The TGA and differential TGA (DTG) curves of the bismaleimide samples under (a, b) nitrogen and (c, d) air; The storage modulus (E') (e) and Tanδ (f) as a function of the temperature of BMI samples

Table 2. TGA data of the bismaleimide samples

Sample	N_2				Air			
	$T_{-10\%}$ (°C)	T_{max} (°C)	$T_{-50\%}$ (°C)	C_{800} (%)	$T_{-10\%}$ (°C)	T_{max1} (°C)	$T_{-50\%}$ (°C)	C_{800} (%)
BMI	423.2	435.4	472.7	27.4	429.8	435.2	549.7	1.7
BMI/MBDPP-1	427.1	439.0	493.9	35.0	428.9	433.6	557.0	0.8
BMI/MBDPP-2	425.0	435.4	613.9	45.5	428.0	433.6	584.5	1.5

3.4 Thermomechanical property

The effect of MBDPP on the thermomechanical property of bismaleimide was studied by DMA. Fig. 3e and 3f shows the storage modulus (E') and Tanδ as a function of the temperature of BMI samples. The glass transition temperature (T_g) is determined by the temperature at the maximum tanδ value. The E' at 30 °C of unmodified bismaleimide was 2159 MPa, while that of BMI/MBDPP-1 and BMI/MBDPP-2 was 2123 and 2487 MPa, respectively. The enhanced E' of BMI/MBDPP-2 was ascribed to the rich aromatic rings in the molecular structure of MBDPP, leading to high rigidity. The crosslinking density (υ_e) was calculated by rubber elastic model theory [24]:

$$\upsilon_e = E'/3RT$$

where E', R and T represent the storage modulus, ideal gas constant (8.314 $J \cdot mol^{-1} \cdot K^{-1}$) and absolute temperature at T_g + 30 °C, respectively. The results are listed in Table 3, showing that the crosslinking density of unmodified BMI, BMI/MBDPP-1 and

BMI/MBDPP-2 was 2.9 × 10^4, 1.4 × 10^4 and 9.6 × 10^3 mol/m^3, respectively. The addition of MBDPP reduced the crosslinking density, which can be explained by the fact that MBDPP has a large steric hindrance, hindering the diffusion rate in the curing reaction, resulting in the decreased crosslinking density as well. Therefore, the T_g of BMI/MBDPP-1 and BMI/MBDPP-2 was decreased to 243 ℃ and 228 ℃, respectively, from 276 ℃ of unmodified BMI. Moreover, the Tanδ curve of BMI showed much broader than those of BMI/MBDPP-1 and BMI/MBDPP-2, suggesting the lower segmental movement in the cured BMI product [22].

Table 3. DMA data of BMI samples

Sample	T_g (℃)	E' (30 ℃) (MPa)	E' (T_g+30 ℃) (MPa)	υ_e (mol/m^3)
BMI	276	2159	415	2.9×10^4
BMI/MBDPP-1	243	2123	179	1.4×10^4
BMI/MBDPP-2	228	2487	131	9.6×10^3

3.5 Flame retardancy

The flame retardancy of BMI and BMI/MBDPP systems were initially evaluated by LOI test and UL-94 vertical combustion test. Table 4 lists the oxygen index (LOI) and UL-94 vertical combustion test results of bismaleimide samples. The LOI of unmodified bismaleimide is 32.0%. In the UL-94 vertical combustion test, it will self-extinguish in 5 s after the first ignition and 13 s after the second ignition (Fig. 4), corresponding to the UL-94 V-1 grade. After flame retardant modification, the LOI of BMI/MBDPP-1 and BMI/MBDPP-2 increases to 34.0% and 35.0%. Generally, if the LOI is beyond 26%, it is considered to be a flame retardant material [25].

BMI/MBDPP-1 and BMI/MBDPP-2 can self-extinguish immediately (≤ 2 s for the ignition twice) in the UL-94 vertical combustion test (Fig. 4), corresponding to UL-94 V-0 grade, indicating that MBDPP has high flame retardant efficiency for BMI.

Table 4. The LOI value and UL-94 classification of BMI, BMI/MBDPP-1 and BMI/MBDPP-2

Sample	LOI (%)	UL-94 (3 mm)		
		t_1+t_2*	Dripping	Classification
BMI	32.0±1.0	5+13	No	V-1
BMI/MBDPP-1	34.0±0.9	1+2	No	V-0
BMI/MBDPP-2	35.0±1.2	1+1	No	V-0

* t_1 and t_2 denote the average combustion time after the first and second ignition, respectively.

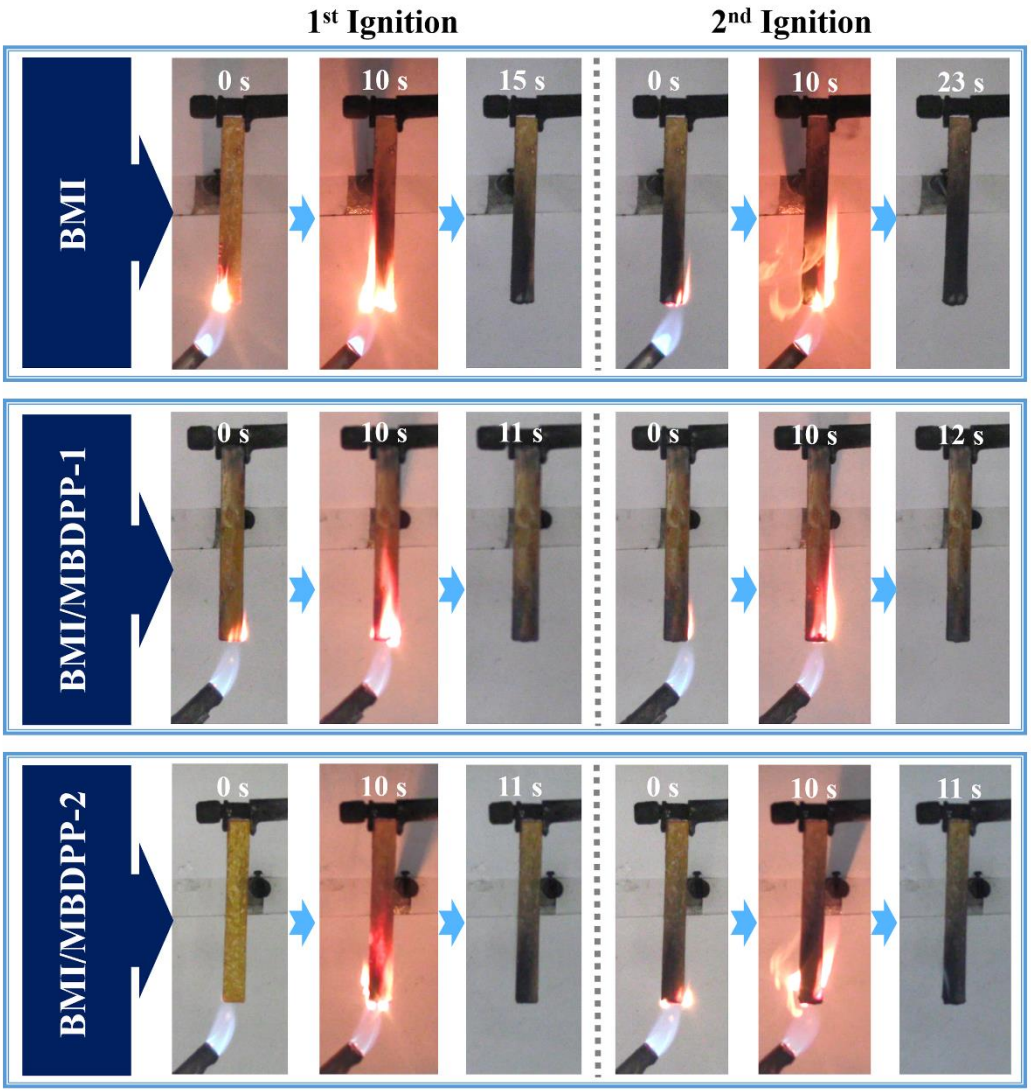

Fig. 4 Screenshots of BMI, BMI/MBDPP-1 and BMI/MBDPP-2 during the UL-94 test procedures. The time includes the exposure time (10 s) for each ignition

The combustion properties of bismaleimide samples were further investigated by a cone calorimeter [26, 27], and the corresponding results are summarized in Fig. 5 and Table 5. Fig. 5a shows a curve of the heat release rate (HRR) of bismaleimide samples with time before and after flame retardant modification. The HRR curve of the unmodified bismaleimide shows a main exothermic peak in the range from 50 to 200 s, and the peak heat release rate (PHRR) reaches 417 kW/m^2, which corresponds to the combustion of the flammable gas released by the degradation of bismaleimide; a secondary exothermic

peak appears in the range from 200 to 400 s, which is due to the formation of a char layer during the combustion. With the continuous rise of temperature, the char layer further oxidizes and decomposes, which cannot continue to prevent the heat release rate, leading to the appearance of the shoulder peak. With the increase of MBDPP addition, the heat release rate peaks of BMI/MBDPP-1 and BMI/MBDPP-2 decreased significantly, especially the value of the second heat release peak decreased significantly, indicating that MBDPP can enhance the thermal stability of the formed char layer, which can significantly inhibit the heat release rate during combustion. Therefore, the PHRR of BMI/MBDPP-1 and BMI/MBDPP-2 was significantly lower than that of unmodified BMI, decreased by 23% and 26%, respectively. The maximum average rate of heat emission (MARHE) is another commonly used parameter to assess the fire spread rate of polymers [28]. From Table 5, it can be seen that the MARHE value declined gradually with increasing the MBDPP loading. The MARHE value of unmodified bismaleimide was 247 kW/m^2. When 1.0 wt% and 2.0 wt% of MBDPP were incorporated, the MARHE values dropped to 188 and 166 kW/m^2, respectively, corresponding to a 24% and 33% reduction.

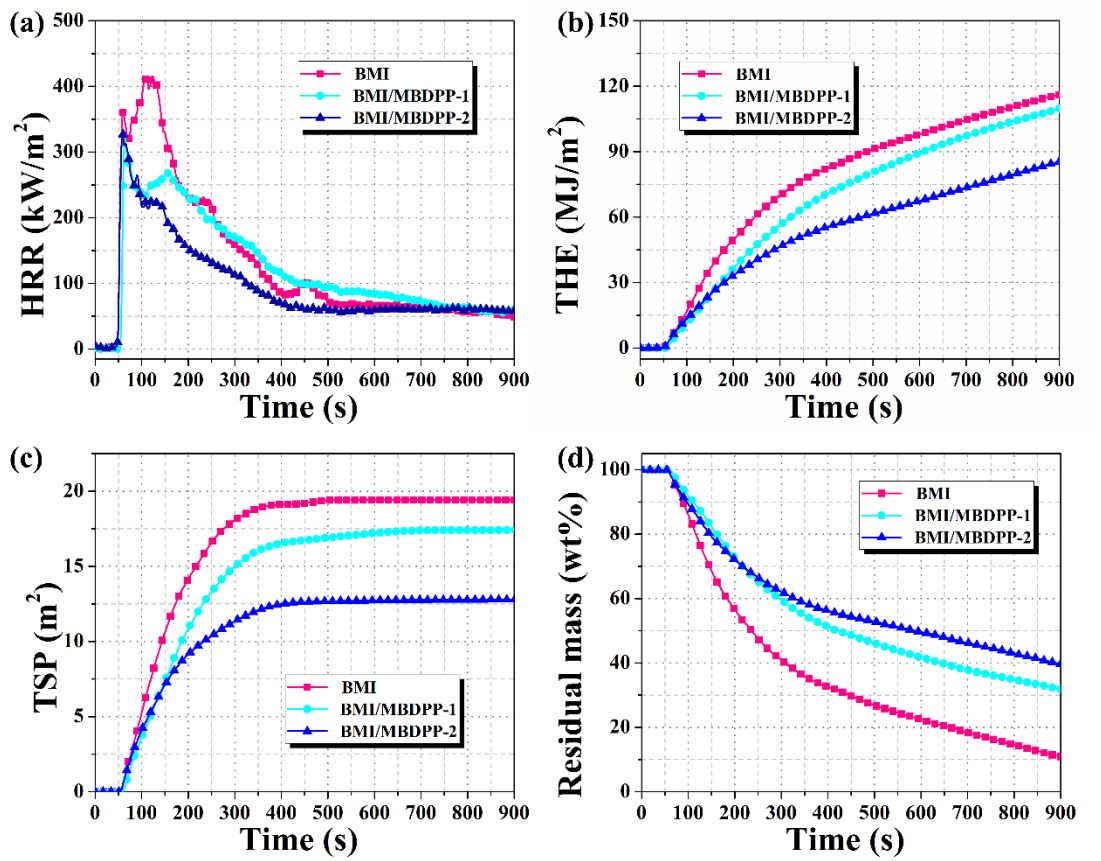

Fig. 5 (a) HRR, (b) THE, (c) TSP, and (d) Mass loss as a function of time plots of bismaleimide samples before and after flame retardant modification

Fig. 5b is the time-dependent curve of total heat evolved (THE) of bismaleimide samples before and after flame retardant modification. The THE of unmodified bismaleimide is 116.8 MJ/m^2, and the THE of BMI/MBDPP-1 and BMI/MBDPP-2 drops to 109.1 and 85.6 MJ/m^2, respectively. This is because the addition of MBDPP can trap polymeric chains in the char residues, resulting in the restriction of fuel to the flame.

Table 5. Cone calorimeter data of the untreated and flame retarded BMI samples

Sample	TTI (s)	PHRR (kW/m^2)	THE (MJ/m^2)	MARHE (kW/m^2)	Mean SEA	TSP (m^2)

					(m^2/kg)	
BMI	54±3.3	417±12.5	116.8±3.8	247±4.7	351±15.0	19.5±0.21
BMI/MBDPP-1	58±2.3	323±10.7	109.1±6.3	188±7.5	305±11.0	17.4±0.47
BMI/MBDPP-2	54±2.9	310±15.5	85.6±4.0	166±3.3	176±7.9	12.8±0.34

Fig. 5c gives the time-dependent curve of total smoke production (TSP) of bismaleimide samples before and after flame retardant modification. The TSP of unmodified bismaleimide was 19.5 m^2, and the TSP of BMI/MBDPP-1 and BMI/MBDPP-2 decreased to 17.4 and 12.8 m^2, respectively. Besides, mean specific extinction area (SEA) is another important index relating to smoke emission during combustion. Compared to unmodified bismaleimide, the mean SEA of BMI/MBDPP-1 and BMI/MBDPP-2 was declined by 13% and 50%, respectively. As aforementioned, more polymeric chains were trapped in the char residues, so the smoke sources were limited.

Fig. 5d is a curve of the mass of bismaleimide samples with time before and after flame retardant modification. It can be seen that BMI/MBDPP-1 and BMI/MBDPP-2 show a slower mass loss process in the whole combustion process compared with unmodified bismaleimide. The char yield of the unmodified bismaleimide after combustion reaches 10.7 wt%, while the char yield of BMI/MBDPP-1 and BMI/MBDPP-2 reaches 31.8 wt% and 39.7 wt%, respectively, indicating that MBDPP can significantly promote the char

forming capacity and thermal stability of the formed char layer during combustion.

3.6 Char analysis

Fig. 6 depicts the side-view and top-view photos of the char residues of (a, b) BMI, (d, e) BMI/MBDPP-1, and (g, h) BMI/MBDPP-2, as well as SEM images of the char residues of (c) BMI, (f) BMI/MBDPP-1 and (i) BMI/MBDPP-2. As can be seen from Figs. 6a and 6b, the char residue of unmodified bismaleimide after combustion is fragmented, and the underlying aluminum foil is also melted under radiation. Under the SEM, the char residue showed a porous morphology (Fig. 6c), which was caused by the escape of pyrolysis products produced by the violent combustion of BMI. After combustion, an expansive char layer was observed for BMI/MBDPP-1 (Fig. 6d and 6e), and the SEM photos showed that the surface of the char layer was dense and continuous (Fig. 6f). For BMI/MBDPP-2, a more compact and expansive char layer was formed (Fig. 6g and 6h), and the SEM photos showed that the surface of the char layer presented a flat and intact morphology (Fig. 6i). The char layer can effectively block the transportation of combustible degradation products to the flame and the thermal radiation of heat to the polymer matrix, so as to slow down the heat release rate.

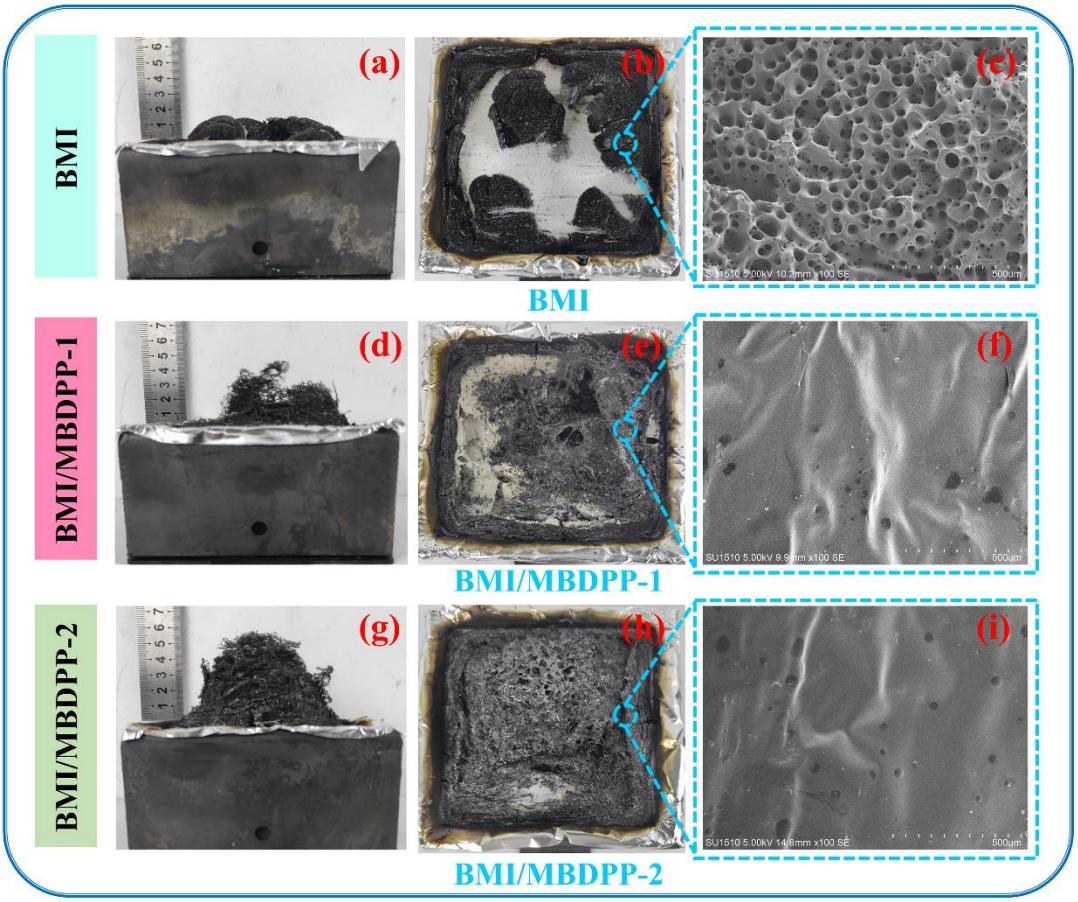

Fig. 6 The side-view and top-view photos of the char residues of (a, b) BMI, (d, e) BMI/MBDPP-1 and (g, h) BMI/MBDPP-2, and SEM images of the char residues of (c) BMI, (f) BMI/MBDPP-1 and (i) BMI/MBDPP-2

The chemical structure of char residue was further analyzed by Raman spectroscopy. Fig. 7a displays the Raman spectra of the residual char of BMI and BMI/MBDPP-2. The Raman spectra of all samples showed two intense characteristic peaks at 1596 and 1360 cm^{-1}, corresponding to the so-called G-band and D-band, respectively. G-band is used to characterize the sp2 crystalline structure of carbon atoms, and D-band reflects the disordered carbon atoms [29]. The ratio of D-band to G-band (I_D/I_G) is a quantitative index to measure the graphitization degree of carbonaceous materials [30, 31]. The higher the I_D/I_G value, the lower content of the graphited carbon atoms. With the

addition of MBDPP, the I_D/I_G value of BMI/MBDPP-2 was decreased to 3.19 from 3.80 for unmodified BMI, indicating that the addition of MBDPP promoted the formation of ordered graphitized char structure, which was conducive to improving the heat resistance of residual char.

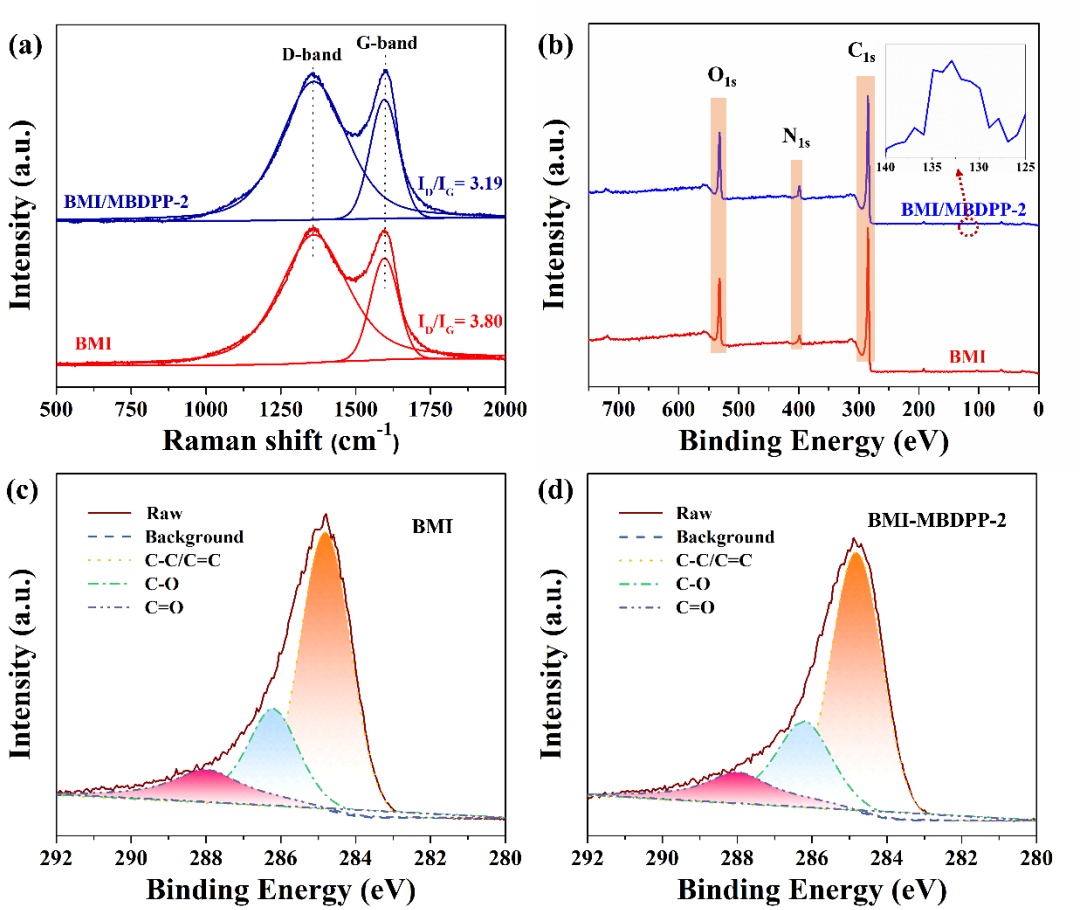

Fig. 7 (a) Raman spectra and (b) full-scan XPS spectra of the residual char of BMI and BMI/MBDPP-2; High-resolution C1s XPS spectra of the char residues of (c) BMI and (d) BMI/MBDPP-2 (Inset image: the partial enlarged view of P2p peak)

The elemental composition of the char residues was further analyzed by XPS [32-35]. Fig. 7b displays the full-scan XPS spectra of the char residues of BMI and BMI/MBDPP-2. The XPS spectrum of the char residue of unmodified BMI showed several strong absorption peaks at 284, 399, and 532 eV, corresponding to carbon,

nitrogen, and oxygen, respectively. Compared with unmodified BMI, the XPS spectrum of the char residue of BMI/MBDPP-2 showed a new absorption peak of P2p at 133 eV. Fig. 7c and 7d show the high-resolution C1s XPS spectra of the char residues of BMI and BMI/MBDPP-2, respectively. The C1s XPS spectra could be deconvoluted into three sub-peaks at 284.8, 286.2, and 288.0 eV, corresponding to aliphatic and aromatic carbon atoms (C-C/C=C), carbon atoms in ether or hydroxyl group (C-O), and carbon atoms in carbonyl or carboxyl group (C=O) [29]. Carbon atoms in C-C/C=C are called non-oxidized carbon (C_a), while carbon atoms in C-O and C=O are called oxygenated carbon (C_{ox}). Generally, the thermal-oxidative resistance of char residues is evaluated by the C_{ox}/C_a ratio [36]. The C_{ox}/C_a ratio of the char residues of BMI and BMI/MBDPP-2 was 0.57 and 0.45, respectively. The C_{ox}/C_a value of BMI/MBDPP-2 was lower than that of BMI, indicating that the char of BMI/MBDPP-2 had better thermal-oxidative resistance. A char layer with excellent thermal-oxidative resistance can provide a better flame retardant effect by inhibiting the diffusion of oxygen and combustible gas and slowing down mass and heat transfer.

3.7 Pyrolysis products evolved analysis

The pyrolysis products evolved were detected by the TGA-FTIR technique [37-40]. Fig. 8a displays the FTIR spectra of BMI at diverse decomposition temperatures. When the temperature rose to 420 °C, several characteristic peaks at 3015, 1715, 1510, 1372, and 1170 cm^{-1} were clearly observed, suggesting the beginning of thermal decomposition. The characteristic peak at 3015 cm^{-1} was assigned to the C-H stretching of aromatic rings. The characteristic peak at 1715 cm^{-1} was allocated to the carbonyl-based species

generated from the decomposition of imide rings [41]. The absorption peaks at 1510 and 1372 cm^{-1} were owing to the skeleton vibration of the aromatic rings and the stretching vibration of the C-N bond, which were pyrolysis products of BDM species [41]. Additionally, the peak at 1170 cm^{-1} was assigned to the C-O bond produced from the pyrolysis of DBA. With the elevated temperature at 440 °C, the absorbance intensity of all the characteristic peaks became strongest, reaching the maximum decomposition stage. When the temperature was beyond 600 °C, the characteristic FTIR signals became weaker and weaker, demonstrating the completion of the major decomposition stage. These results corresponded well with the TGA data. Fig. 8b displays the FTIR spectra of BMI/MBDPP-2 at diverse decomposition temperatures. When the temperature rose to 400 °C, several characteristic peaks at 3015, 2360, 1510, and 1305 cm^{-1} were clearly observed, suggesting the beginning of thermal decomposition. With proceeding the thermal decomposition to 500 °C, the absorbance intensity of these characteristic peaks became more intense, suggesting to reach the maximum decomposition stage. When the temperature was elevated beyond 600 °C, the characteristic peaks at 3015 and 1510 cm^{-1} corresponding to the aromatic compounds were still observed, indicating the much slower pyrolysis of the char residues due to the promoted thermal stability of chars by MBDPP. Fig. 8c and 8d compared the absorbance intensity of the typical decomposition products including carbonyl (1715 cm^{-1}) and aromatic (1510 cm^{-1}) compounds between BMI and BMI/MBDPP-2. It can be found that the absorbance intensity of the typical decomposition products of BMI/MBDPP-2 was much lower than that of BMI. As aforementioned, more polymeric

chains were trapped in the char residues, so the decomposition products entering the gas phase were restrained. Since most of these decomposition products were combustible, the fuel supply was cut off so that the heat release and smoke emission were inhibited.

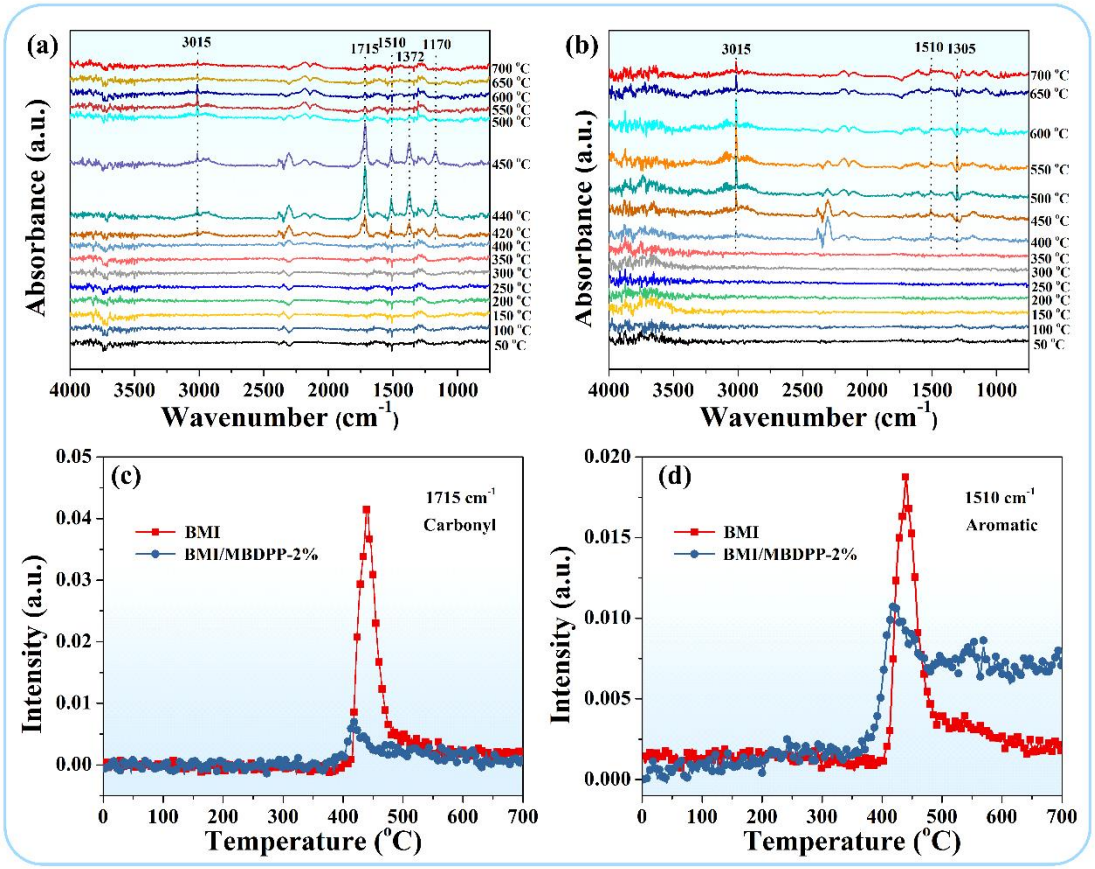

Fig. 8 FTIR spectra of (a) BMI and (b) BMI/MBDPP-2 at diverse decomposition temperatures; Comparison of the absorbance intensity of (c) carbonyl and (d) aromatic compounds between BMI and BMI/MBDPP-2

3.8 Flame retardant mechanism

Based on the char residue and the pyrolysis products evolved analysis, the flame retardant mechanism of MBDPP was proposed as Scheme 2. When heated, MBDPP decomposed to generate phosphoric acid species that enable BMI matrix to dehydrate,

cyclize and carbonize to form an intact, expansive and thermally resistant char layer. The increased char yield means the inhibition of the thermal decomposition process from solid fuel to gas volatiles. Thus, more BMI molecules were trapped in the solid residues (demonstrated by TGA and cone calorimeter results), and less amount of pyrolysis products entered the gas phase to feed the flame (demonstrated by TGA-FTIR results). Since these pyrolysis products are the major sources of fuel and smoke particles, the reduced amount of the pyrolysis products relieved the heat release and smoke emission. Besides, the presence of such a char layer served as a barrier in shielding the BMI matrix from heat irradiation, preventing further fierce decomposition. From the analysis above, the mode of flame retardant action of MBDPP mainly occurred in the condensed phase through the enhanced charring capability.

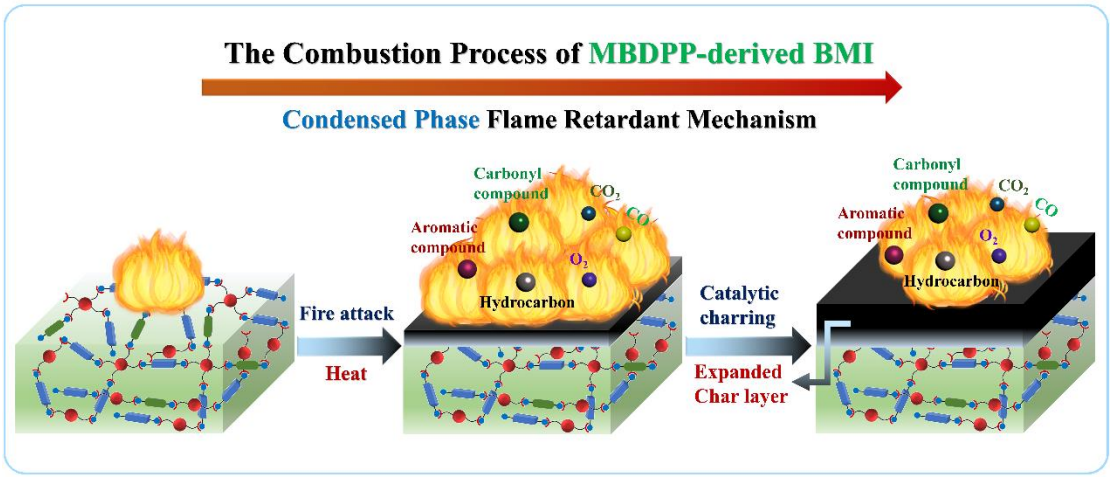

Scheme 2 The flame retardant mechanism of MBDPP

4. Conclusions

In summary, a magnolol-derived bis(diphenyl phosphate) (MBDPP) monomer was successfully synthesized, and then thermally co-polymerized with 2, 2'-diallyl bisphenol A (DBA) and 4, 4'-bismaleimidodiphenylmethane (BDM). The non-

isothermal DSC results indicated that the addition of MBDPP increased the reaction activation energy of the BMI system owing to the steric hindrance of MBDPP. TGA results manifested that the incorporation of MBDPP slightly affected the initial thermal stability of the BMI system, but significantly improved the thermal stability at high temperature and the char yield. The unmodified BMI exhibited an LOI of 32.0% and UL-94 V-1 grade, whereas the BMI containing 1.0 wt% MBDPP achieved an LOI of 34.0% and UL-94 V-0 grade. In addition, the presence of MBDPP notably decreased the PHRR, MARHE, THE, TSP, and mean SEA of the BMI system. The improved anti-flammability and smoke suppression performances of the BMI system were attributable to the formation of an intact, expansive, and thermally resistant char layer that can inhibit the diffusion of oxygen and combustible gas and slow down mass and heat transfer. This study provides a promising and efficient solution to high-performance BMI resins with superior fire safety characteristics.

Acknowledgments This work was supported by the Textile Light Applied Basic Research Project (Grant No.: J202107), the Hong Kong Scholars Program (Grant No.: XJ2020003), the Doctor Project of Innovation and Entrepreneurship in Jiangsu Province (Grant No.: JSSCBS20210821) and the Basic Research Program of Jiangnan University (Grant No.: JUSRP121029).

Conflict of interest The authors declare that they have no conflict of interest.

References

[1] R.J. Iredale, C. Ward, I. Hamerton, Modern advances in bismaleimide resin technology: A 21st century perspective on the chemistry of addition polyimides, Prog.

Polym. Sci. 69 (2017) 1-21.

[2] H. Yao, Z. Fan, H. Cheng, X. Guan, C. Wang, K. Sun, J.Y. Ouyang, Recent development of thermoelectric polymers and composites, Macromol. Rapid Commun. 39 (2018) 1700727.

[3] M. Neda, K. Okinaga, M. Shibata, High-performance bio-based thermosetting resins based on bismaleimide and allyl-etherified eugenol derivatives, Mater. Chem. Phys. 148 (2014) 319-327.

[4] Z. Wang, W. Wu, Y. Zhong, M. Ruan, L.L. Hui, Flame-retardant materials based on phosphorus-containing polyhedral oligomeric silsesquioxane and bismaleimide/diallylbisphenol a with improved thermal resistance and dielectric properties, J. Appl. Polym. Sci. 132 (2015) 41545.

[5] C. Tang, H. Yan, S. Li, M. Li, Z. Chen, Novel phosphorus-containing polyhedral Oligomeric Silsesquioxane functionalized Graphene oxide: preparation and its performance on the mechanical and flame-retardant properties of Bismaleimide composite, J. Polym. Res. 24 (2017) 157.

[6] Y. Wang, X. Jia, H. Shi, J. Hao, H. Qu, J. Wang, Graphene Nanoplatelets Hybrid Flame Retardant Containing Ionic Liquid and Ammonium Polyphosphate for Modified Bismaleimide Resin: Excellent Flame Retardancy, Thermal Stability, Water Resistance and Unique Dielectric Properties, Materials 14 (2021) 6406.

[7] X. Zhou, S. Qiu, W. Cai, L. Liu, Y. Hou, W. Wang, L. Song, X. Wang, Y. Hu, Construction of hierarchical MoS_2@TiO_2 structure for the high performance bimaleimide system with excellent fire safety and mechanical properties, Chem. Eng.

J. 369 (2019) 451-462.

[8] X. Zhou, S. Qiu, J. Liu, M. Zhou, W. Cai, J. Wang, F. Chu, W. Xing, L. Song, Y. Hu, Construction of porous g-C_3N_4@PPZ tubes for high performance BMI resin with enhanced fire safety and toughness, Chem. Eng. J. 401 (2020) 126094.

[9] S. Li, H. Yan, S. Feng, X. Li, Phosphorus-containing flame-retardant bismaleimide resin with high mechanical properties, Polym. Bull. 73 (2016) 3547-3557.

[10] X. Chen, J. Ye, L. Yuan, G. Liang, A.J. Gu, Multi-functional ladderlike polysiloxane: synthesis, characterization and its high performance flame retarding bismaleimide resins with simultaneously improved thermal resistance, dimensional stability and dielectric properties, J. Mater. Chem. A 2 (2014) 7491-7501.

[11] C. Yang, G.Z. Liang, A.J. Gu, L. Yuan, Flame retardancy and mechanism of bismaleimide resins based on a unique inorganic–organic hybridized intumescent flame retardant, Ind. Eng. Chem. Res. 52 (2013) 15075-15087.

[12] X. Zhang, R. Akram, S. Zhang, H. Ma, Z. Wu, D. Wu, Hexa(eugenol) cyclotriphosphazene modified bismaleimide resins with unique thermal stability and flame retardancy, React. Funct. Polym. 113 (2017) 77-84.

[13] X. Zhou, S. Qiu, L. He, X. Wang, Y. Zhu, F. Chu, B. Wang, L. Song, Y. Hu, Synthesis of star-shaped allyl phosphazene small molecules for enhancing fire safety and toughness of high performance BMI resin, Chem. Eng. J. 425 (2021) 130655.

[14] D. Liu, P. Ji, T. Zhang, J. Lv, Y. Cui, A bi-DOPO type of flame retardancy epoxy prepolymer: Synthesis, properties and flame-retardant mechanism, Polym. Degrad. Stabil. 190 (2021) 109629.

[15] Y. Qi, Z. Weng, K. Zhang, J. Wang, S. Zhang, C. Liu, X. Jian, Magnolol-based bio-epoxy resin with acceptable glass transition temperature, processability and flame retardancy, Chem. Eng. J. 387 (2020) 124115.

[16] Y.T. Wu, X.Y. Liu, Z. Tan, Q.X. Zhuang, Synthesis and properties of bio-based benzoxazine resins based on magnolol, Journal of East China University of Science and Technology 46 (2020) 189-196.

[17] Z. Zhang, D. Tian, Z. Niu, Y. Zhou, X. Hou, X. Ma, Enhanced toughness and lowered dielectric loss of reactive POSS modified bismaleimide resin as well as the silica fiber reinforced composites, Polym. Compos. 42 (2021) 6900-6911.

[18] L. Zeng, G. Liang, A. Gu, L. Yuan, D. Zhuo, J. Hu, High performance hybrids based on a novel incompletely condensed polyhedral oligomeric silsesquioxane and bismaleimide resin with improved thermal and dielectric properties, J. Mater. Sci. 47 (2012) 2548-2558.

[19] C. Qu, L. Zhao, D. Wang, H. Li, W. Xiao, C. Yue, Bis [4-(4-maleimidephen-oxy) phenyl] propane/N, N-4, 4′-bismaleimidodiphenylmethyene blend modified with diallyl bisphenol A, J. Appl. Polym. Sci. 131 (2014) 40395.

[20] Y. Qi, Z. Weng, K. Zhang, J. Wang, S. Zhang, C. Liu, X. Jian, Magnolol-based bio-epoxy resin with acceptable glass transition temperature, processability and flame retardancy, Chem. Eng. J. 387 (2020) 124115.

[21] P.S. Balakrishnan, K. Balaji, S.C. Murugavel, Synthesis and chemical curing kinetics of epoxy resin containing α, β-unsaturated carbonyl moiety in the main chain, High Perform. Polym. 23 (2011) 263-270.

[22] H. Nabipour, S. Qiu, X. Wang, L. Song, Y. Hu, Phosphorus-free ellagic acid-derived epoxy thermosets with intrinsic antiflammability and high glass transition temperature, ACS Sustainable Chem. Eng. 9 (2021) 10799-10808.

[23] H. Niu, H. Nabipour, X. Wang, L. Song, Y. Hu, Phosphorus-free vanillin-derived intrinsically flame-retardant epoxy thermoset with extremely low heat release rate and smoke emission, ACS Sustainable Chem. Eng. 9 (2021) 5268-5277.

[24] J. Dai, Y. Peng, N. Teng, Y. Liu, C. Liu, X. Shen, S. Mahmud, J. Zhu, X. Liu, High-performing and fire-resistant biobased epoxy resin from renewable sources, ACS Sustainable Chem. Eng. 6 (2018) 7589-7599.

[25] S.M. Li, J. Ren, H. Yuan, T. Yu, W.Z. Yuan, Weizhong, Influence of ammonium polyphosphate on the flame retardancy and mechanical properties of ramie fiber-reinforced poly (lactic acid) biocomposites, Polym. Int. 59 (2010) 242-248.

[26] X. Wang, Y. Hu, L. Song, H. Yang, B. Yu, B. Kandola, D. Deli, Comparative study on the synergistic effect of POSS and graphene with melamine phosphate on the flame retardance of poly(butylene succinate), Thermochim. Acta 543 (2012) 156-164.

[27] Y. Sun, B. Yuan, S. Shang, H. Zhang, Y. Shi, B. Yu, C. Qi, H. Dong, X. Chen, X. Yang, Surface modification of ammonium polyphosphate by supramolecular assembly for enhancing fire safety properties of polypropylene, Compos. Part B: Eng. 181 (2020) 107588.

[28] Y.Y. Chan, C. Ma, F. Zhou, Y. Hu, B. Schartel, Flame retardant flexible polyurethane foams based on phosphorous soybean-oil polyol and expandable graphite, Polym. Degrad. Stabil. 191 (2021) 109656.

[29] X. Wang, L. Song, H. Yang, W. Xing, B. Kandola, Y. Hu, Simultaneous reduction and surface functionalization of graphene oxide with POSS for reducing fire hazards in epoxy composites, J. Mater. Chem. 22 (2012) 22037-22043.

[30] W. Guo, S. Nie, E.N. Kalali, X. Wang, W. Wang, W. Cai, L. Song, Y. Hu, Construction of SiO_2@ UiO-66 core–shell microarchitectures through covalent linkage as flame retardant and smoke suppressant for epoxy resins, Compos. Part B: Eng. 176 (2019) 107261.

[31] W. Guo, X. Wang, J. Huang, Y. Zhou, W. Cai, J. Wang, L. Song, Y. Hu, Construction of durable flame-retardant and robust superhydrophobic coatings on cotton fabrics for water-oil separation application, Chem. Eng. J. 398 (2020) 125661.

[32] B. Yu, X. Wang, W. Xing, H. Yang, L. Song, Y. Hu, UV-curable functionalized graphene oxide/polyurethane acrylate nanocomposite coatings with enhanced thermal stability and mechanical properties, Ind. Eng. Chem. Res. 51 (2012) 14629-14636.

[33] C.F. Cao, B. Yu, Z.Y. Chen, Y.X. Qu, Y.T. Li, Y.Q. Shi, Z.W. Ma, F.N. Sun, Q.H. Pan, L.C. Tang, Fire intumescent, high-temperature resistant, mechanically flexible graphene oxide network for exceptional fire shielding and ultra-fast fire warning, Nano-Micro Lett. 14 (2022) 1-18.

[34] C.F. Cao, B. Yu, B.F. Guo, W.J. Hu, F.N. Sun, Z.H. Zhang, S.N. Li, W. Wu, L.C. Tang, P. Song, Bio-inspired, sustainable and mechanically robust graphene oxide-based hybrid networks for efficient fire protection and warning, Chem. Eng. J. 439 (2022) 134516.

[35] B. Yuan, Y. Wang, G. Chen, F. Yang, H. Zhang, C. Cao, B. Zuo, Nacre-like

graphene oxide paper bonded with boric acid for fire early-warning sensor, J. Hazard. Mater. 403 (2021) 123645.

[36] X. Wang, S. Zhou, W. Xing, B. Yu, X. Feng, L. Song, Y. Hu, Self-assembly of Ni–Fe layered double hydroxide/graphene hybrids for reducing fire hazard in epoxy composites, J. Mater. Chem. A 1 (2013) 4383-4390.

[37] Z. Zhang, X. Li, Y. Bao, W. Wei, X. Li, X. Liu, Bismaleimide resins modified by an allyl ether of bio-based resveratrol with excellent halogen-free and phosphorus-free intrinsic flame retardancy and ultrahigh glass transition temperature, Polym. Degrad. Stabil. 193 (2021) 109717.

[38] H. Luo, W. Rao, P. Zhao, L. Wang, Y. Liu, C. Yu, An efficient organic/inorganic phosphorus–nitrogen–silicon flame retardant towards low-flammability epoxy resin, Polym. Degrad. Stabil. 178 (2020) 109195.

[39] J. Wang, C. Ma, P. Wang, S. Qiu, W. Cai, Y. Hu, Ultra-low phosphorus loading to achieve the superior flame retardancy of epoxy resin, Polym. Degrad. Stabil. 149 (2018) 119-128.

[40] X. Wang, W. Xing, X. Feng, B. Yu, H. Lu, L. Song, Y. Hu, The effect of metal oxide decorated graphene hybrids on the improved thermal stability and the reduced smoke toxicity in epoxy resins, Chem. Eng. J. 250 (2014) 214-221.

[41] S. Li, H. Yan, C. Tang, S. Niu, Y. Jia, Novel phosphorus-containing polyhedral oligomeric silsesquioxane designed for high-performance flame-retardant bismaleimide resins, J. Polym. Res. 23 (2016) 238.